Cement and Concrete Composites 139 (2023) 105047

Contents lists available at ScienceDirect

Cement and Concrete Composites

journal homepage: www.elsevier.com/locate/cemconcomp

Using Fibre recovered from face mask waste to improve printability in 3D concrete printing

Pathmanathan Rajeev [a,*], Akilesh Ramesh [a], Satheeskumar Navaratnam [b], Jay Sanjayan [a]

[a] Centre for Sustainable Infrastructure and Digital Construction & Department of Civil and Construction Engineering Swinburne University of Technology, Hawthorn, VIC, Australia

[b] School of Engineering, RMIT University, Australia

ARTICLE INFO

Keywords:
3D concrete printing
COVID-19
Face masks
Polypropylene fibres
Flexural strength
Rheology
Interlayer bond strength

ABSTRACT

Surgical face mask usage has rapidly increased in the last two years due to the COVID-19 pandemic. This generates vast amounts of plastic waste, causing significant risks to the ecosystem. Thus, this study assesses the potential of using recycled fibre from face mask waste as fibre reinforcement in 3D concrete printing (3DCP) applications to improve printability while reducing landfill waste. The effect of recycled fibre from waste face masks on the rheological characteristics of printable mixes and the mechanical performance of printed elements was evaluated for different contents of shredded face masks (i.e., 1% and 2% by vol). The rheological properties like static and dynamic yield strengths, apparent viscosity, and thixotropic behaviour, along with compressive and flexural strength, were evaluated for 3D printed specimens and mechanical properties were compared to their mould-cast counterparts. Further, the variation in the interlayer bond strength and porosity due to different fibre dosages was also investigated. In addition, a comparative study on the fresh and hardened properties was performed for the printable mixes with polypropylene (PP) fibres and face masks. The addition of face masks significantly improved the rheological properties with good extrudability and buildability for all the dosages. Compared to face masks, mixes with PP fibres showed poor extrudability with higher fibre dosages. The compressive strength was increased by 41% for a 1% dosage of face masks when compared to the unreinforced concrete. Furthermore, the flexural strength when tested along the weaker interface, showed an increase of 74% and 82% for the addition of 1% and 2% face mask content. The interlayer bond strength of 1% face mask content showed 21% improvement and was observed to have the highest surface moisture content. The mechanical performance of face masks and PP fibres are observed to be comparable for 1% dosage. The mechanical properties of printed and mould-cast specimens were also observed to be similar.

1. Introduction

The need for plastic products has increased significantly in modern society, which raises various environmental concerns. Higher use of various plastic products leads to large plastic debris, and it has low biodegradability, which will create various environmental pollution when it is not properly disposed [1]. Due to the COVID-19 outbreak, an increase in the usage of various single-use plastic products like face masks, face shields and gloves was observed, whereas proper disposal of these wastes is not effective and practical, which causes environmental pollution [2]. Further, the global market for face masks was estimated to exceed $22 billion in 2023 [3] due to COVID-19. This significant increase in the manufacturing of face masks also impacts CO_2 emissions and global warming [4]. Further, the population of face mask waste generated per day is 6600 million, weighing 2640.79 tonnes [5]. Currently, most of this waste is incinerated or disinfected on the same collection day [6]. However, the collection and disposal of facemask waste from the domestic and household sector are proved to be more challenging. More awareness programs, providing separate collection bins for face mask waste and a proper centralised disposal system are some of the strategies suggested for the effective collection and utilisation or disposal of face mask waste [2,3,6,7]. The face mask litter also impact the ecosystem, causing entanglement and may lead to the death of birds and animals. The face masks also get into the aquatic environment and create plastic pollution. Plastic absorbs toxins that poison aquatic creatures when ingested [8]. Hence, the potential ways to

* Corresponding author.
E-mail address: prajeev@swin.edu.au (P. Rajeev).

https://doi.org/10.1016/j.cemconcomp.2023.105047
Received 9 November 2022; Received in revised form 14 February 2023; Accepted 22 March 2023
Available online 6 April 2023

reuse face masks have become a major concern in reducing the environmental impact. The method of integrating natural fibres in producing face masks as a sustainable approach and incorporating mask waste in construction materials are some feasible alternatives in waste management [6].

The most widely used face masks are single-use surgical face masks. Their use is not limited to the COVID-19 pandemic alone, as they are regularly used in the medical field, pharmaceutical companies and the chemical industry. The surgical face mask mainly contains polypropylene, and the addition of polypropylene fibres in concrete reduces the shrinkage cracks and improves fire performance [9]. Koniorczyk et al. [10] suggested a recycling process that heated the used face mask at 190 °C with 130 bar, enabling complete inactivation of the virus and conversion into homogeneous polypropylene strings. This indicates there is a feasibility of using this polypropylene in concrete technology. Further, Saberian et al. [11] investigated various properties of pavement base or subbase when shredded face masks were added. Their study found that the addition of various dosages of face masks with recycled aggregates enhanced the strength, stiffness, ductility and flexibility of the mixes. A recent study by Kilmartin-Lynch et al. [12] investigates the potential of using face masks in concrete. The results showed an increase in compressive strength and tensile strength for lower percentages of face masks. Another study on using face masks in mortar showed an improvement in mechanical performance and thermal resistance [13]. These previous studies indicate that there is a potential to utilise face masks as a substituent for polypropylene fibres. Therefore, the use of face masks as fibre reinforcement for 3D concrete printing applications can be expected to enhance the mechanical properties of printed structures.

Extrusion-based 3D concrete printing is a commonly used additive manufacturing technique that deposits the concrete in a layer-by-layer pattern through extrusion via a nozzle and forms solid elements without the use of formwork [14]. Despite having the advantage of performing freeform construction with 3D concrete printing, its widespread application is hindered by developing good printable concrete and providing reinforcement for structural application [15]. 3D-printed concrete structures are strong in compression but weak in tension, similar to conventional concrete. Also, the interfaces between subsequent layers and filaments form weaker zones when subjected to tensile loading [16]. To enhance the performance of 3D printed structures under tension and flexure, adding short fibres with varying lengths, content and type was evaluated in different studies [17,18]. The addition of fibres was observed to improve the flexural behaviour of 3D printed elements. Furthermore, using natural fibres as reinforcement in 3D concrete printing also improves the mechanical properties and pave way for sustainable green construction [19].

The rheological properties of concrete mix play a vital role in 3D concrete printing to achieve uniform extrusion and improved buildability (i.e., the printable materials are expected to have lower initial yield strength for easy pumping and increasing over time at a higher rate for increased buildability [20,21]). Unlike conventional concrete, 3D-printed concrete needs to focus more on the rheological properties, hydration and fresh state strength [22]. In order to improve the pumpability, the application of vibrational energy around the extruder to reduce the extrusion pressure and initial yield strength was investigated as a feasible active rheology control method [23]. Also, the effect of yield stress on buildability was evaluated both experimentally and numerically extensively elsewhere (e.g., Ref. [24]). Furthermore, to improve the printability and buildability of highly fluid ready mix concrete, a secondary mixing method with the addition of a viscosity modifying agent and recycled coarse aggregates as an onsite approach was evaluated based on the rheological parameters [25].

Furthermore, 3D concrete printing is a free-form construction technique, and as a result, the printed elements are susceptible to high shrinkage cracks [26,27]. This shrinkage crack can be reduced by adding polypropylene fibres, which subsequently improve the mechanical performance of printed elements. Moelich et al. [26] studied various mitigating measures for early-age shrinkage of 3D printed specimens and demonstrated that the addition of short polypropylene fibres effectively reduced the shrinkage cracks without affecting the printing performance. Further, the effect on viscosity and dynamic yield strength for suitable printing with low shrinkage with the addition of polypropylene fibres was evaluated by Tran et al. [28], and the study showed adding polypropylene fibres considerably influences the rheological properties and reduces the shrinkage cracks. Van Der Putten et al. [27] developed 3D printable concrete by studying the effect of different lengths and dosages of polypropylene fibres. A reduction in the workability was observed with increasing fibre dosage, whereas the flexural strength was improved, and the shrinkage was reduced. The influence of fibre orientation on the flexural behaviour and shrinkage of 3D concrete printed members with polypropylene fibres was evaluated by Ma et al. [29] and the results showed that adding polypropylene fibres not only improved flexural strength but also reduced shrinkage due to the better orientation of fibres along the printing direction.

These previous research studies highlighted that adding polypropylene fibres to the 3D printed concrete help to improve its printability, shrinkage and mechanical performance. This indicates the potential to use the polypropylene generated as a recycled fibre from face mask waste. Therefore, this study aims to assess the feasibility of developing a sustainable fibre reinforced 3D printed concrete using shredded face masks. To achieve this, the objectives of this research were divided into two sections: (1) evaluate the rheological and early-age mechanical properties of concrete mixes with varying fibre dosages of shredded face masks (i.e., 1% and 2% by volume) and (2) evaluate the compressive strength, flexural strength and interlayer bond strength performance of 3D printed specimens with shredded face masks fibre. To study the anisotropic behaviour of 3D printed elements due to printing direction to the loading conditions, the pure compression and three-point bending tests were performed on various specimens considering three different directions of printing. Further, the apparent porosity was evaluated to analyse the void percentage from the addition of fibres and, the results were compared with printed and mould-cast specimens with commercially available polypropylene fibres.

2. Materials and mix preparation

2.1. Concrete

The binder for the printable concrete mix used in this study consists of Ordinary Portland cement (OPC) agreeing to AS 3972 [30] and silica fume agreeing to AS 3582.3 [31]. Three different sieve-graded silica sands, categorised as fine sand, medium sand, and coarse sand, with mean particle sizes of 224 μm, 460 μm, and 879 μm, respectively, were used as aggregates. Sieve analysis was carried out to obtain the particle size distribution of sands as per ASTM C136 [32], while laser ultrasonic technique was used for OPC and silica fume. Fig. 1 shows the particle size distribution of all dry materials.

Further, a polycarboxylate ether (PCE) based superplasticiser (SP) (MasterGlenium SKY 8379) in liquid form was used to adjust the workability of the mix. To delay the cement hydration and ensure a sufficient open time for the mix, a retarder (MasterSet RT 122) was used. Both the admixtures conform to AS 1478.1 [33] standards.

2.2. Short fibres

Surgical face masks (FM) and commercially available polypropylene (PP) fibres were used in this study for performance comparison. Due to the safety regulations of our laboratory, waste face masks were not permitted to be used. Further, Koniorczyk et al. [10] study highlighted no significant changes in the chemical moieties of recycled and used masks. Thus, to assess the feasibility of using FM in the 3DCP, this study used clean surgical face masks. The clean surgical face masks that were

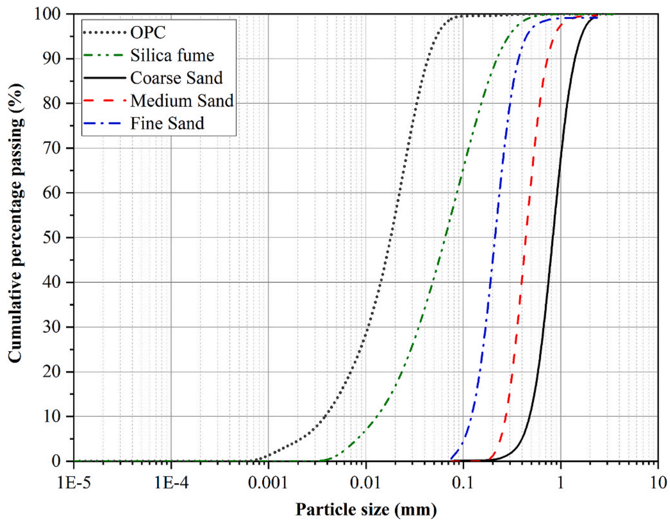

Fig. 1. Particle size distribution for graded sands.

cut into a length of 6 mm and a width of 1 mm were used (Fig. 2b). The metallic nose strip and the elastic ear loops of FM were removed. Face masks are comprised of three layers, a non-woven fabric on top and bottom, with a meltdown PP in the middle [6]. The details of the surgical face mask adopted in this study are given in Fig. 2a. The short PP fibres used in this study are commercially available and have a length of 6 mm. The properties of FM and PP fibres are given in Table 1. A uni-axial tensile test as per ASTM D5035-11 [34] was performed on the cut face mask to determine its tensile strength and modulus of elasticity. Three samples of FM which were cut into strips 1 mm wide and 150 mm long, were tested in a uni-axial tensile test under a constant displacement rate of 0.5 mm/min. The samples were gripped at both ends of the testing machine with an aluminium plate. The test setup used in this study and the stress-strain behaviour of the FM fibre is given in Fig. 3.

2.3. Mix preparation

The mix proportion adopted for all the different mixes used in the study is illustrated in Table 2. All the dry materials (including the fibres) were weighed and added to a planetary mixer. The fibres were added as volume fractions. The dry materials were mixed slowly for about 2 min for homogeneous dispersion of the fibres and the materials. Then, half of the water was mixed with SP and retarder and was added slowly to the mixer and continued mixing at a slow speed (i.e., 70 rpm) for 5 min. The remaining water was added slowly while mixing at the same speed and continuing mixing for 3 min. Finally, the mixing was continued for five more minutes at high speed (i.e., 190 rpm). Further, the control mix was formulated to achieve the required rheology by optimising the SP and retarder ratio for printing. In addition, the fibre dosage adopted in this study was based on printability and strength requirements. Higher fibre dosages result in difficulty during extrusion, whereas lower dosages result in a lack of strength improvement. Furthermore, as suggested by previous researchers [19,36–38], 1% and 2% fibre content can be used to assess the strength and printability performance of 3D-printed concrete.

Table 1
Properties of face mask and PP fibres.

Type	Length (mm)	Diameter/ width (mm)	Tensile strength (N/ mm^2)	Elastic modulus (MPa)
FM	6	1	29.5 ± 3.0 (i.e., coefficient of variation = 10.2%)	265.3 ± 20.0 (i.e., coefficient of variation = 7.5%)
PP[a]	6	0.018	557	4158

[a] Provided by the supplier [35].

3. Experimental program

3.1. Specimen preparation

The gantry-type 3D printer having a working space of 1.8 m length, 1.6 m width and 1.8 m height used in this study is shown in Fig. 4a. Fig. 4b shows the auger type extruder placed on the actuator of the printer. The X, Y and Z directional movement of the printer was monitored using a customised computer program. A feeder was attached to the extruder for adding the concrete mix to the extruder. A 30 mm diameter removable nozzle was connected at the extruder outlet. The printing speed was adopted as 30 mm/s, and the auger rotation speed was adjusted from 0.6 rad/s to 0.8 rad/s to maintain uniform extrusion of the printed filaments.

Two sets of solid slabs having a dimension of 360 mm × 400 mm were printed as shown in Fig. 5 for each mix in which one slab consisted of four layers, and the other had five layers. Each layer consists of multiple adjacent filaments and has a layer thickness of 10 mm each. Adjusting the extrusion rate by regulating the rotation speed of the auger resulted in uniformly printed filaments. The printed slab showing the printing path is shown in Fig. 5. These printed slabs were saw-cut to the required dimensions of prisms and cubes for testing the hardened

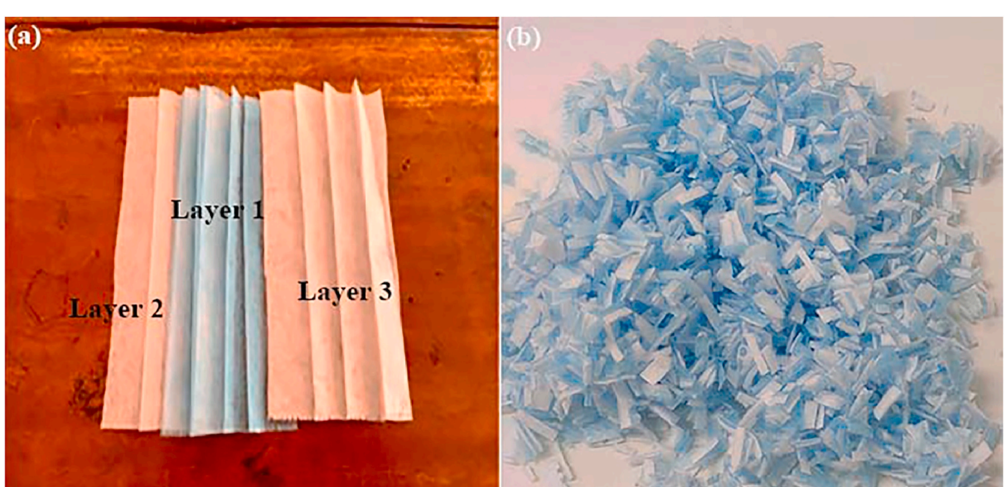

Fig. 2. Surgical face masks: (a) Three layers in a surgical face mask [6]; (b) shredded FM.

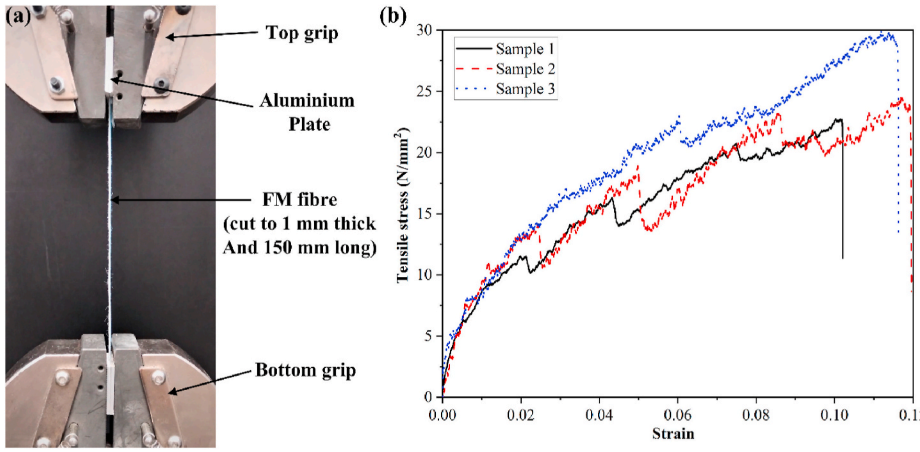

Fig. 3. (a) Tensile test setup for FM; (b) Stress-strain relation of FM.

Table 2
Mix proportion.

Mix ID	OPC	Silica fume	Fine sand	Medium sand	Coarse sand	Water	SP[a] (%)	Retarder[a] (%)	Fibres[b] (%)
CM-0FM-0PP	0.8	0.2	0.5	0.5	0.5	0.28	0.4	0.35	0
CM-1FM-0PP	0.8	0.2	0.5	0.5	0.5	0.28	0.4	0.35	1
CM-2FM-0PP	0.8	0.2	0.5	0.5	0.5	0.28	0.4	0.35	2
CM-0FM-1PP	0.8	0.2	0.5	0.5	0.5	0.28	0.4	0.35	1
CM-0FM-2PP	0.8	0.2	0.5	0.5	0.5	0.28	0.4	0.35	2

Note: Mix ID represents the following, CM, FM, and PP stand for control mix, face mask and polypropylene fibre respectively. The mix CM-1FM-0PP represents a control mix with a 1% volume fraction of face mask and no polypropylene fibres.

[a] Superplasticizers and retarders are % by weight of the binders.

[b] Fibre content is shown as the volume fraction.

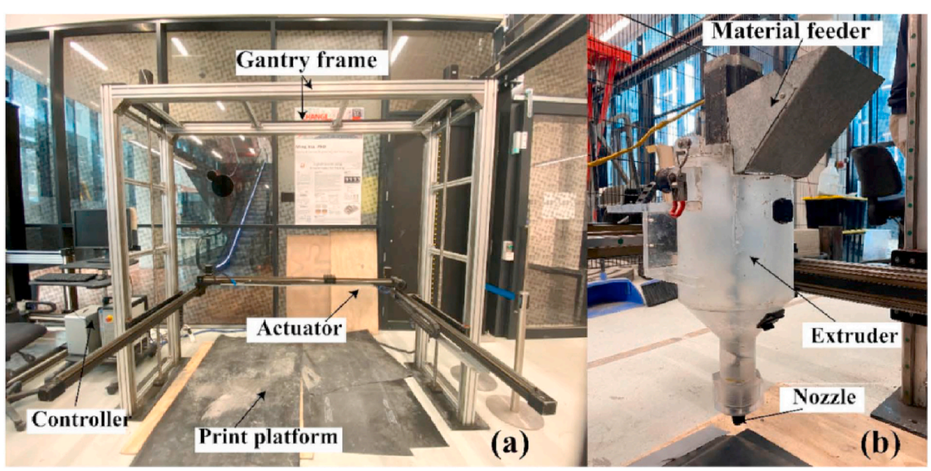

Fig. 4. 3D printing system: (a) 3D printer; and (b) Auger type extruder [36].

properties. Similarly, the prisms and cubes were prepared for the five mixes by mould-cast method to compare with the printed specimen. The mix was poured slowly into the mould and was vibrated approximately for 2 min using a vibration table for good compaction. Both the printed and mould-cast specimens were covered for 24 h to avoid moisture loss and then were cured in the water, maintaining the temperature at 23 ± 0.5 °C until the test period was reached.

3.1.1. Fresh properties

The workability of printable mixes was measured from the average of the two perpendicular spread diameters using the flow table test as per ASTM C1437 [39]. The spread diameters were measured before and after 25 drops of the flow table. For measuring the rheological properties of the mixes, a rotational rheometer (Viskomat XL) was used as shown in Fig. 6. A six-blade vane having 69 mm height and 34.5 mm radius was immersed into the rheometer vessel (diameter 135 mm and height 170 mm) filled with fresh concrete. To measure the torque, only the vessel is rotated as per the applied shearing protocol while the vane remains still. The extended Reiner-Riwlin equation was adopted to obtain the shear stress, shear rate and viscosity from the torque and rpm [40]. A steel cage was used to avoid the slippage of concrete from the inner face of the vessel. Further, a visual inspection was carried out to prevent errors in plug flow and fibre migration while using a rotational rheometer and confirmed that no plug cavities and fibre migration were observed. Furthermore, three measurements were conducted for each mix, and an average of the results are reported to avoid anomalies in the data due to

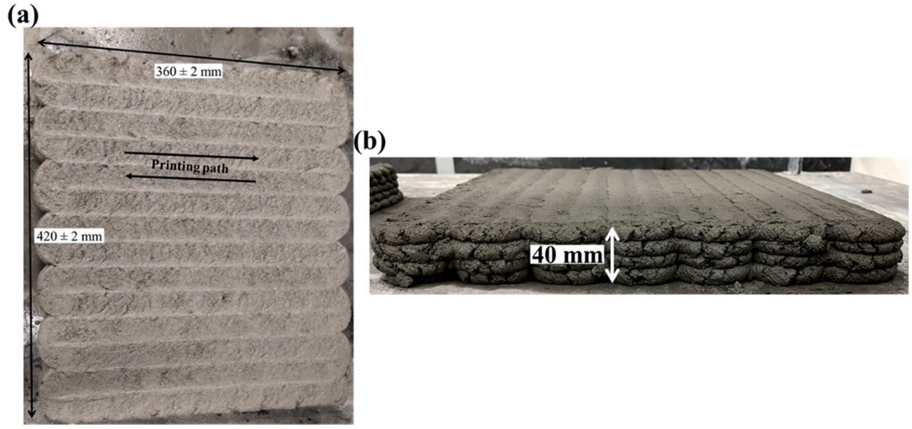

Fig. 5. 3D printed slab specimens: (a) Top view; and (b) Front view.

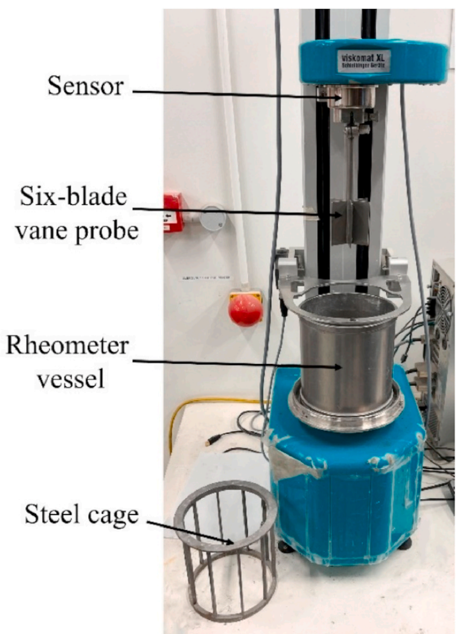

Fig. 6. Rheometer with six-blade vane and steel cage.

non-homogeneity. For all the mix proportions, the same batch of the concrete mix prepared for the printing process was used for accessing the rheological parameters using the rotational rheometer.

3.1.2. *Apparent viscosity*

The variation in the pumpability of the concrete due to the addition of fibres was evaluated based on the changes in the viscosity of the mix. During the pumping process, a thin lubricating layer around the inner surface of the pipe is formed for easy propagation of the concrete [41]. Hence, in the calculation of viscosity, the effect of the lubricating layer needs to be included. However, separating this layer and evaluating the viscosity can be very difficult. Thus in this study, the rheological parameters of the concrete are considered as a whole in evaluating the pumpability of the mix [42]. The flow curve was used to evaluate the apparent viscosity and dynamic yield strength of the mixes. Fig. 7a shows the shearing behaviour adopted to determine the flow curve for all the mixes. Further, the mixes were pre-sheared before beginning the shearing protocol to avoid any differences during the transfer period. The maximum shearing rate of 6.45 s^{-1} is achieved in the step of 0.8065 s^{-1} and then reduced to zero. The shear rate increase in each step was retained for 30 s to reach a constant state, and thus the total flow curve is for about 7.5 min. The average value of the shear stress calculated corresponding to the last 5 s of each step was used as the shear stress to that shear rate. The apparent viscosity and dynamic yield strength of the fresh concrete were calculated from the downward section of the flow curve [43]. The flow behaviour of the concrete mix can be characterised by viscosity and dynamic yield strength, thus giving an insight into the pumpability.

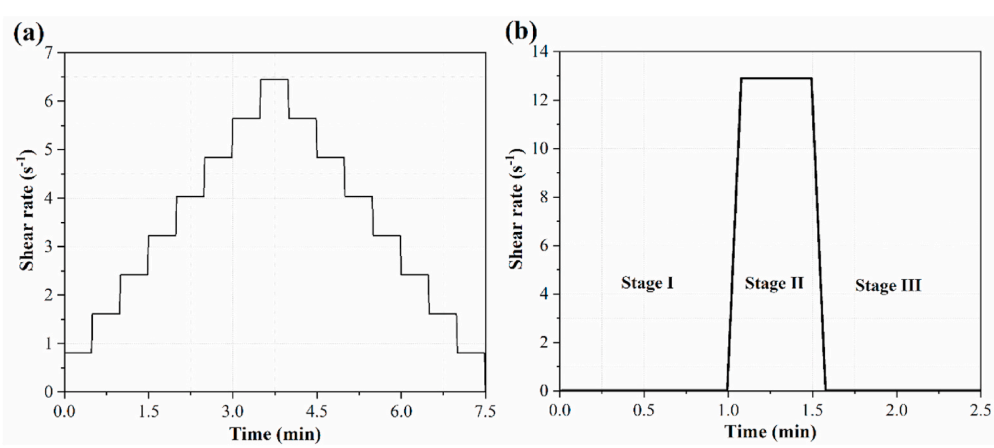

Fig. 7. Shearing protocol for: (a) Flow curve; (b) viscosity recovery behaviour.

3.1.3. Viscosity recovery after extrusion

A decrease in the viscosity of the concrete mix under shearing and recovery similar to the initial viscosity when shearing stops, is referred to as thixotropy [44]. The thixotropic behaviour of the printable mixes was understood by adopting a three-stage shearing protocol as shown in Fig. 7b. Initially, the fresh mix will be at rest before feeding and is represented by a 0.01 s^{-1} shear rate in the shearing protocol. Further, during the 3D printing process, the fresh concrete mix is sheared by the auger while getting extruded, which reduces the viscosity. However, the actual shearing condition of the concrete during extrusion is affected due to various factors like distance between the vane and cylinder, the effect of nozzle walls and non-uniform shearing by the screw-type auger [42]. Hence a high shearing rate of 13 s^{-1} (which is the upper limit of Viskomat XL) was applied in the second stage to assume complete shearing of the mix. Finally, after deposition, the shearing is removed represented by the low shear rate of 0.01 s^{-1} in the third stage. The deposited concrete mix should recover to its initial state so the layers can retain their shape. High viscosity at this stage represents good shape retention ability of the mix, which is good for printing.

3.1.4. Elastic behaviour under fresh state

The elastic behaviour of the concrete mixes was investigated by performing a stress ramp test in the rheometer. A constant stress rate from 0 to 9000 Pa was applied to the mix for 37 min to measure the resultant strain. The applied shear ramp rate was similar to the real-time printing condition [20]. The mix is in an elastic state until failure, which is represented by the drop in the applied stress [45]. The shear ramp rate is determined from the following Equation (1).

$$Shear\ ramp\ rate = \frac{\rho \times g \times h}{t} \tag{1}$$

where ρ is the density of concrete, g is the gravitational constant, h is the height of the printed structure, and t is the time to complete printing.

3.1.5. Yield strength measurement over time

The buildability of the mix is another important factor that has a significant role in the performance of 3D concrete printing. Hence, it is important to analyse the variation in the buildability of the mixes with the addition of fibres with different types and contents. To characterise the buildability of the mix, rheological properties are measured as a quantitative evaluation method. Generally, the fresh concrete mix is assumed to fail either due to material failure or stability failure [46]. Material failure of the fresh concrete is due to the plastic yielding, whereas stability failure which corresponds to buckling failure mainly resembles the stiffness of the concrete [47]. To avoid material failure, the concrete mix should always have sufficiently higher static yield strength than the gravity-induced stresses from the subsequent layers. Thus, the static yield strength development over time was measured in this study to investigate the material failure. Measurement of static yield strength development of the mixes can be performed with a rheometer. However, a significant difference was observed in the yield strength results for a single batch mix approach and a multiple batch mix approach, where the single batch mix underestimates the yield strength [42]. Furthermore, the multiple batch mix approach is a time consuming process, hence the penetrometer test was adopted in this study to determine the yield strength development over time. In this method, a needle is attached to the load cell and is steered at a slow speed into the fresh concrete and the resistance given by the concrete during penetration was measured [48]. Fig. 8 shows the schematic and experimental setup for the penetrometer test used in this study. The static yield strength of the concrete is measured based on Equation (2) [49].

$$\tau_o = \frac{F}{\pi R \sqrt{R^2 + h^2}} \tag{2}$$

where F is the resisted force in N *and* R and h represents the radius and height in mm of the needle cone respectively. A total of three tests were conducted for each mix, and the loading rate was kept very slow at 0.166 mm/min and the test was conducted for 30 min for each mix.

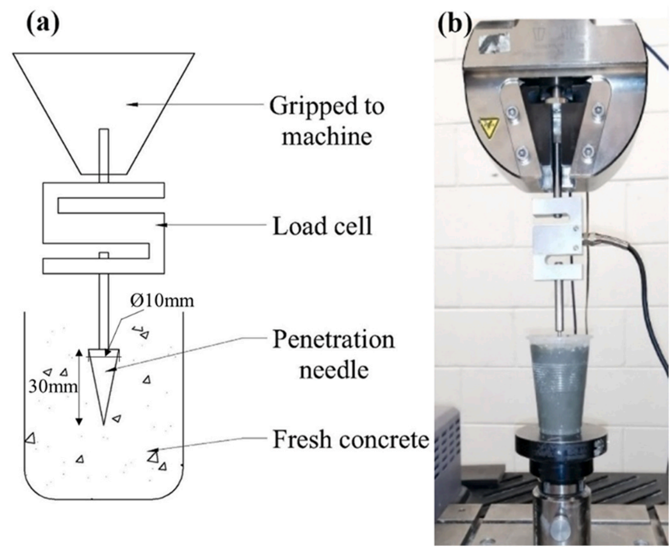

Fig. 8. Penetrometer test setup: (a) schematic diagram; and (b) experiment setup.

3.2. Hardened properties

The printed solid slabs with five layers were saw-cut into 50 × 50 × 50 mm cubes and cured till testing until 7 and 28 days under compression. To study the anisotropic behaviour of the printed specimens, a total of nine cubes (Fig. 9a) were tested for each mix (3 cubes for each direction) for both 7 and 28 days. A constant loading rate of 0.33 $N/mm^2/s$ was applied during the pure compression test. Similarly, six mould-cast cubes of 50 × 50 × 50 mm for each mix were tested under compression at 7 and 28 days. The printed slabs with four layers were saw-cut into 40 × 40 × 160 mm prisms to evaluate the flexural strength under three-point bending after curing at 7 and 28 days. To evaluate the effect of printing direction on flexural strength, three prisms were tested for each direction for all the mixes (Fig. 9b). The flexural testing of prisms was conducted under a constant displacement rate of 0.5 mm/min. To compare the mould-cast flexural strength, six 40 × 40 × 160 mm prisms were cast and tested in bending at 7 and 28 days.

3.2.1. Interlayer bond strength

To understand the strength between the printed layers, a total of 12 specimens having dimensions 40 × 40 × 40 mm were saw-cut from the 4-layer printed solid slab for each mix. To evaluate the pull-out load between the layers at failure, each sample was tested under a uni-axial tensile test under a constant displacement rate of 0.5 mm/min at 7 and 28 days. A small notch of 5 mm in depth is created at the location of the interlayer (i.e., between the second and third layer) to create the failure at the interlayer plane [43,48,50]. The notch having 5 mm depth in a triangular shape was prepared manually using a saw-cutting machine on both sides of the specimen and care was taken to avoid damaging the sample during preparation. Metallic brackets clamp the samples to the testing machine on the top and bottom (Fig. 10). The interlayer bond strength is calculated as the pull-out load divided by the contact area.

The interlayer bond strength depends on the surface moisture content of the printed filaments [50]. Hence, the surface moisture content of printed filaments for different mixes was calculated using the cut-to-size paper method suggested in previous studies for printed specimens [50, 51]. A paper of 250 mm long and 20 mm wide was placed on the top

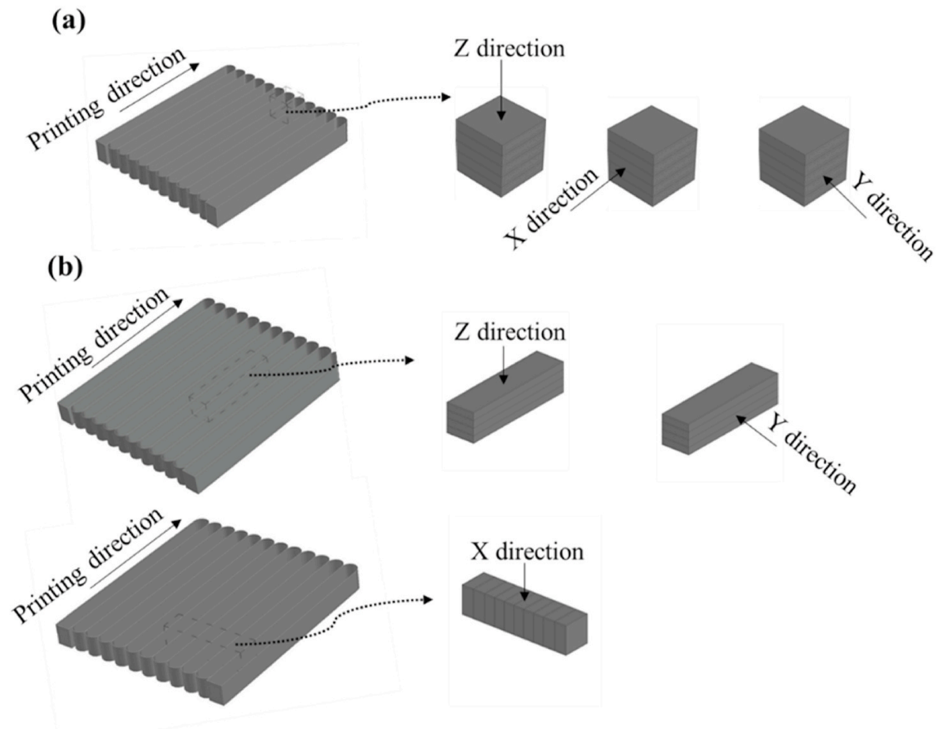

Fig. 9. Schematic representation of saw cut specimens and different printing directions: (a) compression test specimens; and (b) flexural test specimens.

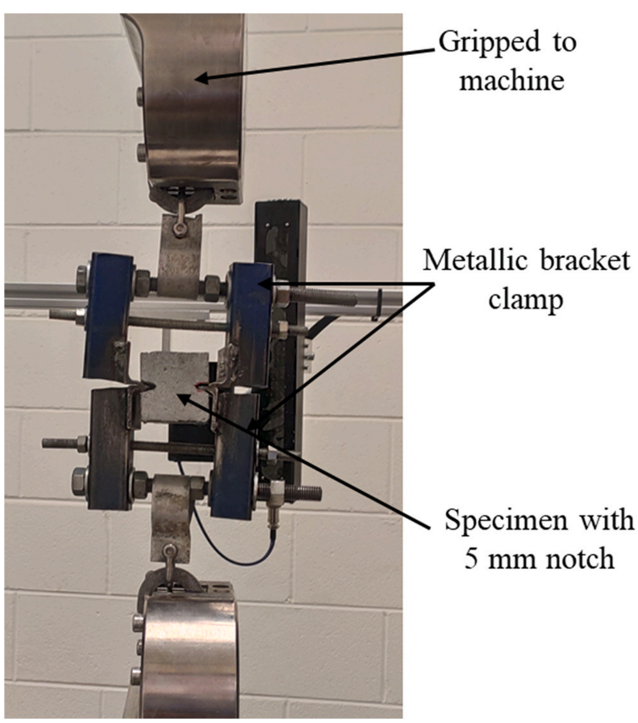

Fig. 10. Interlayer bond strength test setup.

surface of the printed filament having a dimension of 250 mm × 30 mm × 10 mm to absorb the moisture. The initial weight of the paper was measured and after placing the paper for 20 s on the printed surface, they were removed carefully, and the weight gain was calculated. Three samples were used for each mix and the average weight gain was measured. The experiment was conducted in a controlled environment of 25 °C and 50% relative humidity.

3.2.2. Volume of permeable voids

The mechanical performance of the concrete mixes depended on the voids present and was evaluated by determining the void percentage using ASTM C642 [52] of all the mixes for both mould-cast and 3D printed specimens. Three specimens having dimensions of 40 × 40 × 40 mm were cut from the flexural samples and tested for measuring void percentage after 28 days. The dry weight (W_1) was measured after oven-drying the specimens at 105 °C for one day. The specimens were allowed to cool down to ambient temperature before measuring the weight. Later on, the specimens were immersed in water for one day to measure the saturated surface dry weight (W_2). Further, the specimens were immersed in boiling water for 5 h to measure the boiled surface dry weight (W_3). Finally, for measuring the apparent mass (W_4) the specimens were suspended in water. All the weights were measured in grams. The percentage volume of permeable voids (V) was determined using Equation (3).

$$V = \frac{W_3 - W_1}{W_3 - W_4} \times 100\% \tag{3}$$

4. Results and discussion

4.1. Workability of concrete mixes

Fig. 11 shows the spread diameter for different mixes before and after drops of the flow table test. The diameter before the drop was similar to the cone bottom diameter (100 mm). Hence, the mixes showed low slump; thus, measuring flow diameter at different time intervals is difficult. An increase in the spread diameter from the initial can be observed after 25 drops of the flow table but still within the range of 123–148 mm, which was suitable for a printable mix [21,53]. Furthermore, it was observed that the workability of the mixes was reduced by adding fibres, thus resulting in higher pumping pressure. Compared to FM fibres, the mixes having PP fibres showed slightly lower workability for the same fibre content. This could be attributed to more clogging of the PP fibres due to low diameter compared to FM fibres.

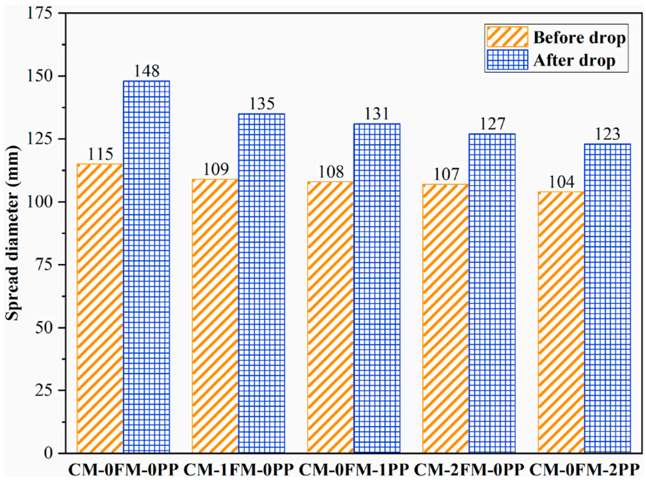

Fig. 11. Spread diameters before and after 25 drops of the flow table.

4.2. Apparent viscosity

Fig. 12 shows the plot of shear stress vs shear rate for all the mixes fitted to the modified Bingham model. The control mix showed no significant increase in shear stress with an increase in shear rate. However, mixes with fibres showed increased shear stress with shear rate, and the effect was significant for 2% fibre content. This indicates that adding fibres will increase the viscosity of the mixes, which results in creating stiffer mixes that need higher torque to be applied for shearing and thus results in higher shear stress with an increase in shear rate [54]. The increase in shear stress with shear rate indicates the behaviour to be shear-thickening, which is common for cementitious mortars and concrete [55]. Compared to FM fibres, adding PP fibres tend to increase the viscosity and makes the mix stiffer and thus has higher shear stress than adding FM fibres in the mix. This can be attributed to the more flexible nature of FM fibres compared to that of PP fibres. This further reduces the overall friction between the particles resulting in lower shear stress [56].

The apparent viscosity and dynamic yield strength at different shear rates for all the mixes are shown in Figs. 13 and 14, respectively. The apparent viscosity reduces significantly as the shear rate increases, irrespective of the mixes (Fig. 13). The addition of fibres increases the apparent viscosity, which can be due to the adhesive nature of the fibre and matrix interface [57]. For lower shear rates, both FM fibre and PP

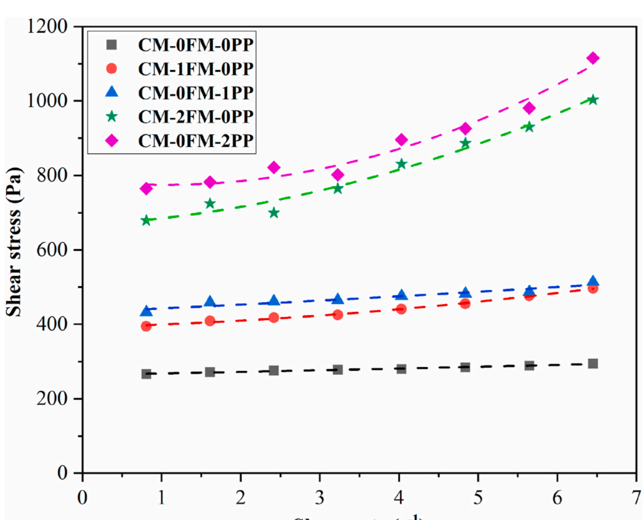

Fig. 12. Flow curves of all the mixes (curve fitted to modified Bingham model).

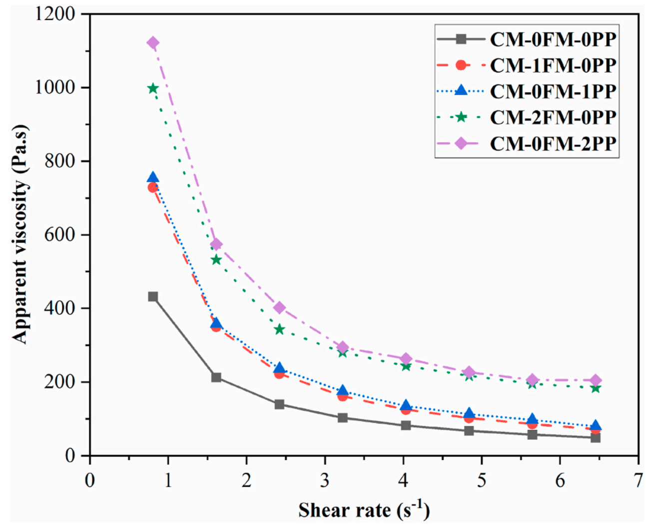

Fig. 13. Apparent viscosity vs shear rate.

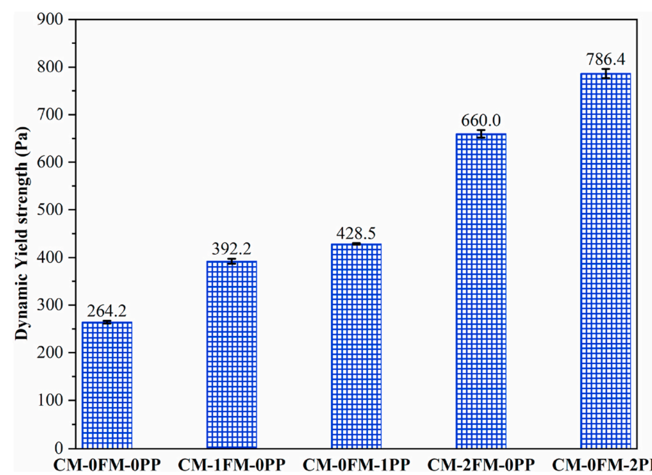

Fig. 14. Dynamic yield strength (error bar indicates mean ± one standard deviation).

fibre mixes had higher apparent viscosity than the control mix. In the case of CM-1FM-0PP (i.e., mix with 1% FM) and CM-0FM-1PP (i.e., mix with 1% PP) mixes, as the shear rate increases, the apparent viscosity is reduced to ~ 10^2 Pa s which was close to the control mix. The lower viscosity at higher shearing can be attributed to improving the pumpability. The pumpability can also be characterised based on the dynamic yield strength value and the yield strength value should be less than 1300 Pa for a smooth pumping of the mix [42]. Fig. 14 shows that the yield strength increased when the fibre contents of both FM and PP increased. Compared to CM-2FM-0PP (i.e., mix with 2% FM), the concrete mix CM-0FM-2PP (i.e., mix with 2% PP) showed higher dynamic yield strength, which induces constraints in the pumping.

4.3. Thixotropy and elastic behaviour of fresh mix

Based on analysing the viscosity recovery of the mixes subjected to the three-stage shearing protocol as explained in section 3.2.2, a similar viscosity change was observed for all the mixes (Fig. 15). Furthermore, irrespective of fibre contents, all the mixes showed high viscosity in the initial resting period and low viscosity (i.e., less than 10^2 Pa s) under the application of high shear during extrusion. All the mixes except the CM-0FM-2PP mix showed an excellent recovery rate (i.e., around 95%) at the third stage, which represents the better printing condition of the mix

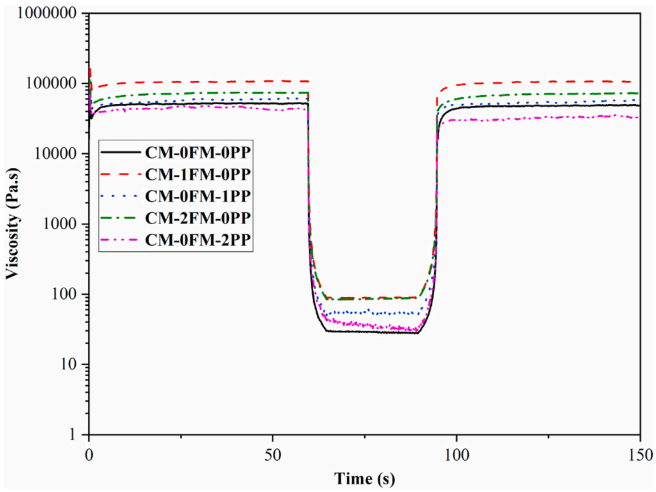

Fig. 15. Viscosity recovery results of all mixes.

after extrusion. The CM-0FM-2PP mix showed a low recovery rate (i.e., about 80%), which can be due to the high friction offered by the fibre matrix at the extruder interface resulting in non-uniform deposition while printing. Even though the viscosity is high for the CM-0FM-2PP mix, high shearing during the second stage disperses the fibres resulting in low viscosity values. The CM-1FM-0PP mix showed the highest recovery rate, which resembles uniform printability with excellent shape retention and this can be due to the better flexibility of the face mask fibres.

The elastic modulus of the fresh mix was derived from the stress vs strain graph obtained in the shear ramp test (Fig. 16). It was observed that the addition of fibres to the mix increased the stiffness, resulting in a higher elastic modulus. Furthermore, an increase in the elastic modulus of the mixes containing fibres results in good buildability while printing. In addition, the elastic modulus of FM fibre mixes was 0.67 MPa and 0.99 MPa, respectively for CM-1FM-0PP and CM-2FM-0PP mixes. This indicates that the mix has good rigidity and shows better resistance to buckling failure. Furthermore, the addition of PP fibres offers higher stiffness to the fresh mix and thus increases the elastic modulus significantly. Compared to the mixes with FM fibres, the mixes with PP fibres showed higher elastic modulus and an increase of 5% and 11% in the elastic modulus was observed for 1% and 2% content of PP fibres, respectively over similar fibre content of FM fibres.

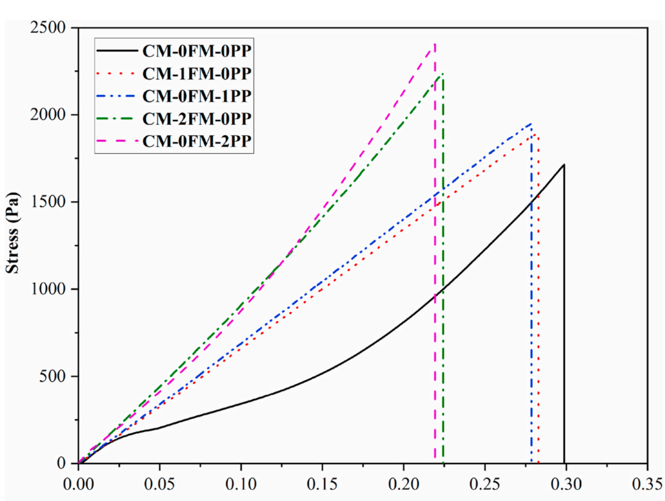

Fig. 16. Fresh concrete elastic behaviour of all mixes.

4.4. Development of static yield strength

The yield strength growth with time for all the mixes is shown in Fig. 17. It can be observed that with an increase in fibre content for both the FM and PP fibres, the rate of increase of yield strength is higher compared to the control mix. However, compared to FM fibres the yield strength development was higher for PP fibres with increasing fibre content. This can be due to the increased stiffness created by the PP fibre and matrix interlocking or entangling of the fibres [56]. This effect can be higher when the fibre content is increased, which can be seen in the CM-0FM-2PP mix (Fig. 17). The higher yield strength shows good buildability for PP fibre mixes, but a sudden increase in the yield strength for higher contents can result in poor extrudability.

The effect of adding FM fibres on the yield strength growth is more significant after 15 min for 1% fibre content and 6 min for 2% fibre content. The overall rate of yield strength over time is also gradual for FM mixes, which suggests not only good buildability but also good extrudability. This study was limited to 30 min as this period can be considered as a critical printing period [20,48]. Further, the effect of the hydration of cement on the yield strength can be discarded as the mixes contain a retarder [20]. Other studies also observed a similar yield strength trend when adding PP fibres [56]. However, the effect of fibre content on the static yield strength growth clearly depicts that compared to difficulties of entangling PP fibres on higher contents, FM fibres show gradual growth, and the surface structure of FM fibres gives less stiffness resulting in more cohesive printing.

4.5. Effect of FM and PP fibres on the hardened properties

Figs. 18 and 19 represent the compressive strength at 7 and 28 days, respectively for both mould-cast and 3D printed samples. The compressive strength of the mould-cast specimens was observed to be increased by 16% and 41% at 7 and 28 days, respectively for 1% FM fibre mix. However, the addition of more FM fibres did not significantly improve the compressive strength of the mix. The gain in compressive strength for the CM-2FM-0PP mix compared to the CM-1FM-0PP mix was 3.8% and 4.5% at 7 and 28 days, respectively. This behaviour was observed because of the formation of voids due to the excess amount of fibres and also due to the presence of different layers in FM, which distributes randomly in concrete. Adding face masks in concrete showed similar trends in compressive strength by Ajam et al. [13]. Moreover, adding 1% PP fibre to the mix gave the highest compressive strength for mould-cast specimens. An increase in compressive strength of 37% and 48% for 7 and 28 days, respectively was observed for the CM-0FM-1PP

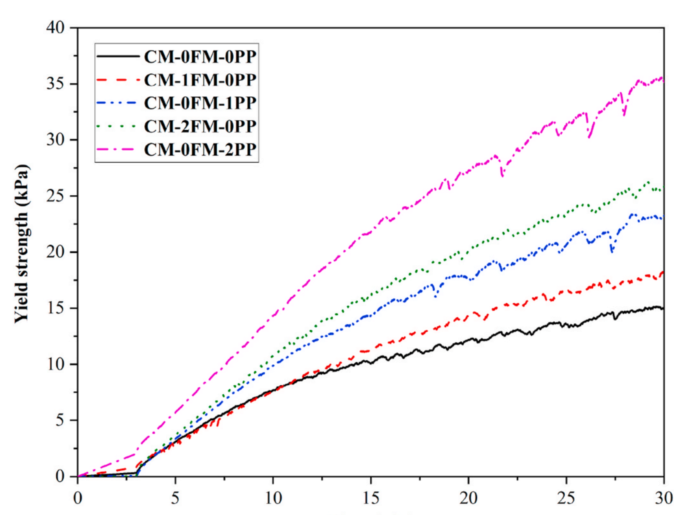

Fig. 17. Static yield strength development of different mixes.

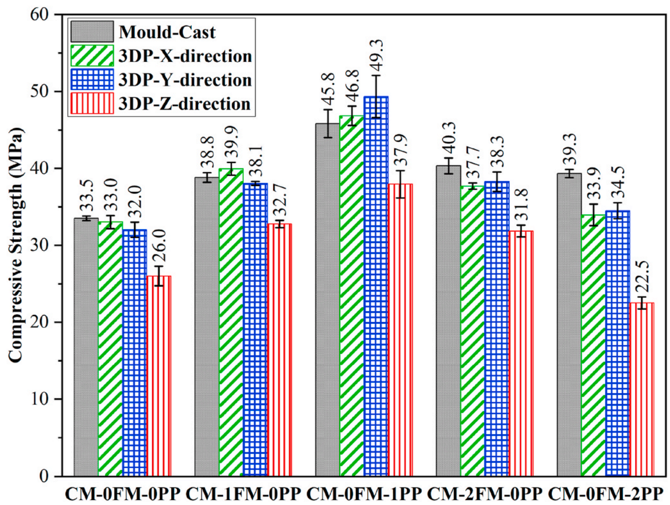

Fig. 18. Compressive strength at 7 days of all the mixes (error bar indicates mean ± one standard deviation).

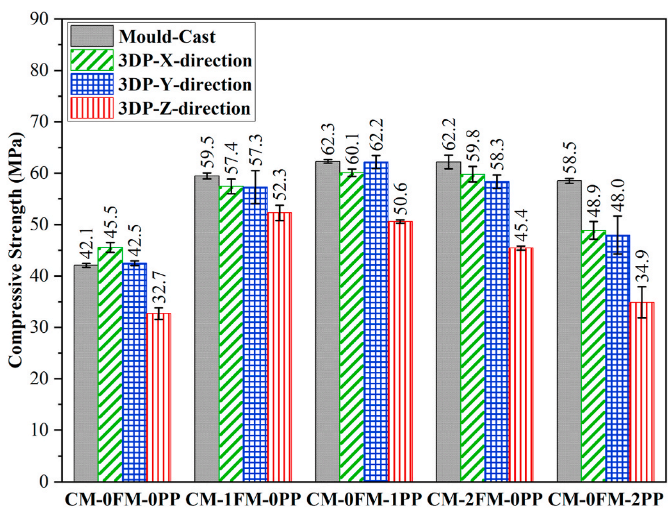

Fig. 19. Compressive strength at 28 days of all the mixes (error bar indicates mean ± one standard deviation).

mix. This can be attributed to the uniform distribution of the fibres and the higher tensile strength of PP fibres compared to FM, which reduces the micro cracks leading to increased compressive strength. Similar behaviour was not observed for the CM-0FM-2PP mix. The addition of 2% PP fibre content reduced the workability, which creates more pores and thus resulted in reduced compressive strength than the 1% PP fibre content mix. Similar behaviour was observed by other researchers with a higher dosage of PP fibres [56].

Unlike the mould-cast specimens for 3D printed specimens, the loading direction corresponding to the printing pattern affects the compressive strength of the mix. Similar behaviour is observed for both 7 and 28 days specimens. 3D printed specimens tested along the X-direction and Y-direction gave close results to the mould-cast specimens. During the extrusion through the nozzle, the printed layers are compacted without any additional vibration. However, the specimens tested along the Z-direction gave the least compressive strength. Similar anisotropic behaviour of 3D printed specimens is observed by several researchers [17,36]. Further, adding FM fibres resulted in increased compressive strength along all the loading directions, whereas the addition of PP fibres from 1% to 2% showed a reduced compressive strength. The trend was similar to mould-cast specimens, however, the reduction was higher for the printed specimens. This can be compared to the rheological characteristics of the 2% PP fibre mix. The addition of 2% PP fibres significantly increased the mix's viscosity and yield strength, resulting in non-uniform extrusion, creating higher pores, and reducing the compressive strength. However, unlike PP fibres, adding FM fibres showed incremental behaviour on the compressive strength of the mix.

Similar to the compressive strength, the 3D-printed specimens loading direction with respect to printing also affects the flexural behaviour. Figs. 20 and 21 show the flexural strength of all the mixes at 7 and 28 days, respectively.

The flexural strength of the mould-cast specimens increased as fibre content increased, irrespective of the fibre type. The addition of fibres increased the cracking load and delayed the crack formation. Unlike the sudden brittle failure of the control mix, a softening behaviour under flexure was observed for both FM fibres and PP fibres. The flexural strength of the CM-1FM-0PP mix and the CM-0FM-1PP mix was observed to be similar for both 7 and 28 days. This reflects that at 1% fibre content, both fibres get dispersed uniformly and enhance the composite action under bending. The residual strength after cracking was observed to be higher for PP fibres than FM fibres. This was mainly due to the higher tensile strength of PP fibres compared to FM fibres. Furthermore, the different layers of the face mask may not be uniformly distributed to resist the complete load, resulting in lower residual strength of the FM mixes.

The 3D-printed specimens showed different flexural strengths along different loading directions than mould-cast specimens. However, specimens tested along the Z-direction (perpendicular to printing) gave the highest flexural strength due to better fibre orientation. In all the mixes, specimens tested along the X-direction gave the lowest flexural strength. This is mainly due to the weak interface of the printed filaments aligning along the loading direction. Moreover, it can be observed that the addition of 1% and 2% of FM fibres increased flexural strength by about 60% when tested along the X-direction. This shows that FM fibres enhance the interface bond strength between filaments. Compared to FM fibres, when 2% PP fibres were added, the flexural strength was reduced in all directions. This can be explained based on the high viscosity of the CM-0FM-2PP mix, which disrupts the smooth extrusion, resulting in more pores and thus reducing the strength. Similar behaviour was observed for the 2% PP fibre mix on the compressive strength results. The enhanced hardened properties of the mixes with FM fibres show their potential as a substitute for PP fibres. A further detailed study needs to be performed to understand the behaviour of FM fibres to establish their potential.

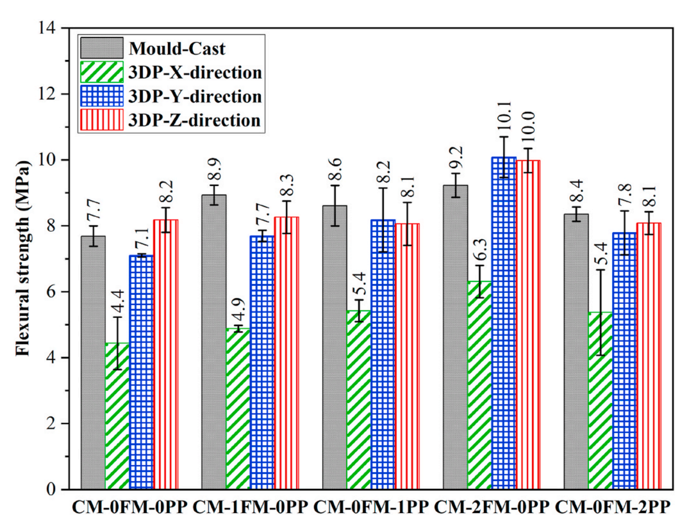

Fig. 20. Flexural strength of all the mixes at 7 days (error bar indicates mean ± one standard deviation).

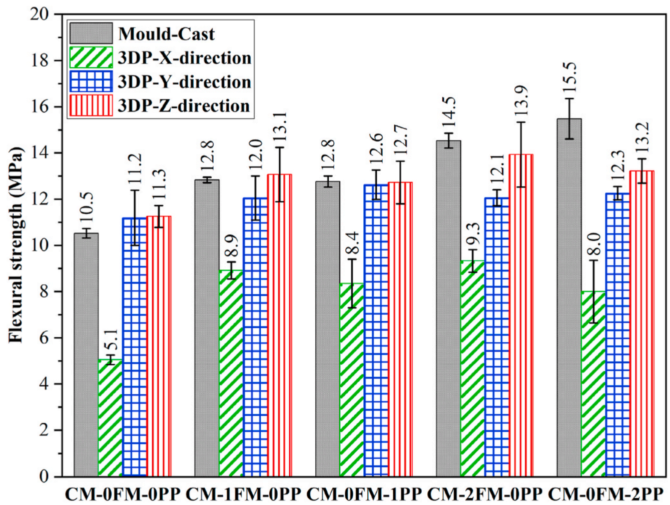

Fig. 21. Flexural strength of all the mixes at 28 days (error bar indicates mean ± one standard deviation).

4.6. Interlayer bond strength

3D concrete printing adopts layer-by-layer deposition of material; hence, the strength between the interlayer is important for using 3D-printed structures for practical applications. The interlayer bond strength determined for all the mixes is given in Fig. 22. An increase in the interlayer bond strength with age was observed for all the mixes and the highest bond strength of 1.65 MPa (with a coefficient of variation = 4.9%) was observed for the CM-1FM-0PP mix at 28 days. However, the addition of fibres of more than 1% dosage was observed to reduce the bond strength. The reduction in the bond strength can be attributed to lower surface moisture content. The variation in the surface moisture of all the mixes is also shown in Fig. 22. It can be observed that as fibre content increases, the viscosity of the mix increases resulting in reduced surface moisture content. With a lower surface moisture content, the subsequent layer adhesion gets reduced. This behaviour was clearly observed for the CM-0FM-2PP mix, as the bond strength at 28 days was reduced by 45% when compared to the control mix. Whereas the CM-2FM-0PP mix showed similar bond strength to the control mix. When comparing the interlayer bond strength of the mixes, FM shows reasonably good performance, and the bond strength was sufficient to avoid interlayer shear failure during flexural testing.

4.7. Volume of permeable voids

When compared to the mould-cast specimens, 3D printed specimens showed slightly lower mechanical properties, especially with higher fibre dosages. When the fibre content of the mix increases, the viscosity and yield strength of the mixes is increased, which reduces the flowability and increases the chance of creating voids. This was analysed by measuring the percentage volume of permeable voids of the mixes for both 3D-printed and mould-cast specimens which are shown in Fig. 23. It can be observed that as fibre content increases, the void percentage of the mix increases for both mould-cast and printed specimens. However, for mixes CM-0FM-0PP and CM-1FM-0PP, the void percentage is similar for both 3D-printed and mould-cast specimens. This indicates that the 3D-printed mixes had good extrudability, which resulted in uniform printing and from the auger pressure achieved good compaction similar to mould-cast specimens. Irrespective of the fibre type and content all the 3D-printed specimens had higher void percentages when compared to their mould-cast counterparts as the mould-cast specimens were compacted better by vibration. A significant increase in the volume of voids was observed for the CM-0FM-2PP mix, which shows a reduction in the mechanical performance of the mix. The viscosity and yield strength of CM-0FM-2PP fibres were higher and as a result, even vibration did not improve the compaction of the mix, which resulted in a higher void percentage.

5. Conclusions

This paper focused on investigating the performance of shredded face masks for 3D concrete printing applications. The addition of face masks as short fibres by 1% and 2% by volume to 3D printed concrete affects both the printing performance as well as mechanical behaviour. Comparing the performance of face masks with commercially available PP fibres showed the potential for using face masks as a substitute for PP fibres in 3D concrete printing applications. Based on the experimental study, the following key outcomes were derived.

- The addition of face masks in 3D printable concrete mix affects the rheological behaviour significantly. An increase in apparent viscosity and dynamic yield strength was observed when face masks were added to the control printable mix. Even though dynamic yield strength increases with fibre content, the face mask mixes showed good extrudability and were within the pumpability range.
- 3D printed specimens with 1% face masks improved the compressive strength by 41% at 28 days, and specimens tested in X and Y

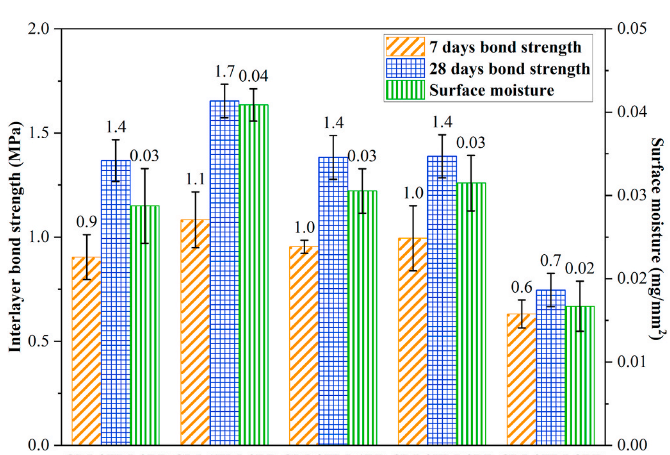

Fig. 22. Interlayer bond strength at 7 days and 28 days and surface moisture of 3D printed specimens (error bar indicates mean ± one standard deviation).

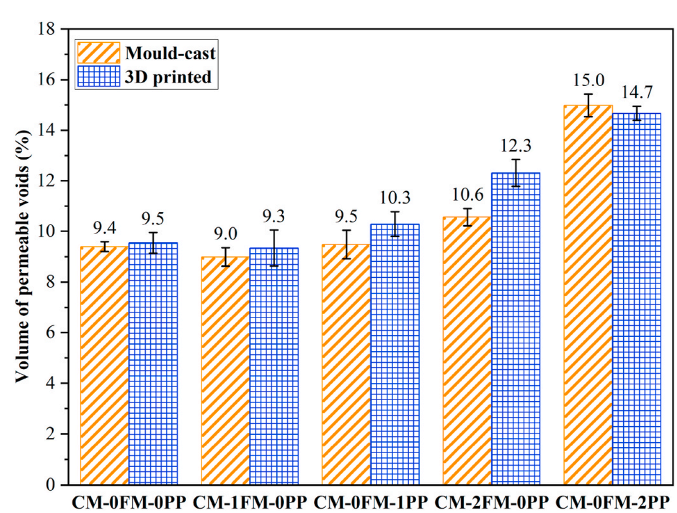

Fig. 23. Volume of permeable voids (error bar indicates mean ± one standard deviation).

directions showed similar results to mould-cast specimens. Further increase in the face mask content reduced the compressive strength. Whereas, the flexural strength of the printed specimen showed significant improvement for both 1% and 2% content of face masks. Furthermore, 3D-printed specimens tested along the X-direction which has the weaker interface section showed an increase in flexural strength at 28 days by 74% and 82% with the addition of 1% and 2% face masks, respectively.
- Interlayer bond strength was increased for 1% fibre content of face masks, but further increase in face mask dosage reduces the surface moisture between the layers and thus reduces the interlayer bond strength.
- A comparison of face masks with commercial PP fibres showed that printable mixes with face masks showed similar rheological behaviour for 1% fibre content. With an increase in fibre dosage, the face mask mixes did not show a sudden increase in viscosity and yield strength. However, mixes with PP fibres showed higher viscosity and yield strength which results in difficulty during extrusion.
- The compressive and flexural strengths of mixes CM-1FM-0PP and CM-0FM-1PP showed similar behaviour. However, with an increase of fibre content to 2% resulted in reduced compressive and flexural strength, especially for the PP fibre mix.
- The reduction in mechanical behaviour was consistent with the void percentage measurements. The addition of fibres increased the volume of voids, and CM-0FM-2PP showed the highest void percentage. Compared to mould-cast specimens, 3D-printed specimens showed higher voids due to the presence of an interface between print filaments.

Declaration of competing interest

The authors declare that they have no known competing financial interests or personal relationships that could have appeared to influence the work reported in this paper.

Data availability

Data will be made available on request.

Acknowledgements

Authors gratefully acknowledge the financial support from the Australian Research Council Grant DP210101680 and LE170100168 for the research work reported in this paper. Further, the authors are greatly thankful to the staff of the Digital Construction Laboratory at the Swinburne University of Technology.

References

[1] F.G. Torres, G.E. De-la-Torre, Face mask waste generation and management during the COVID-19 pandemic: an overview and the Peruvian case, Sci. Total Environ. 786 (2021), 147628.
[2] M.B. Alfonso, et al., Assessing threats, regulations, and strategies to abate plastic pollution in LAC beaches during COVID-19 pandemic, Ocean Coast Manag. 208 (2021), 105613.
[3] Y.T. Tesfaldet, et al., Assessing Face Mask Littering in Urban Environments and Policy Implications: the Case of Bangkok, vol. 806, Science of The Total Environment, 2022, 150952.
[4] T. Liebsch, The Rise of the Face Mask: What's the Environmental Impact of 17 Million N95 Masks, Ecochain, 2020. www.ecochain.com.
[5] M. Idrees, et al., Recycling of waste facial masks as a construction material, a step towards sustainability, Materials 15 (5) (2022) 1810.
[6] K. Selvaranjan, et al., Environmental challenges induced by extensive use of face masks during COVID-19: a review and potential solutions, Environ. Challenge. 3 (2021), 100039.
[7] N. Asim, M. Badiei, K. Sopian, Review of the valorization options for the proper disposal of face masks during the COVID-19 pandemic, Environ. Technol. Innovat. 23 (2021) 101797.
[8] G. Ferraro, P. Failler, Governing plastic pollution in the oceans: institutional challenges and areas for action, Environ. Sci. Pol. 112 (2020) 453–460.
[9] X. Liu, et al., On the mechanism of polypropylene fibres in preventing fire spalling in self-compacting and high-performance cement paste, Cement Concr. Res. 38 (4) (2008) 487–499.
[10] M. Koniorczyk, et al., Performance of concrete containing recycled masks used for personal protection during coronavirus pandemic, Construct. Build. Mater. 324 (2022), 126712.
[11] M. Saberian, et al., Repurposing of COVID-19 single-use face masks for pavements base/subbase, Sci. Total Environ. 769 (2021), 145527.
[12] S. Kilmartin-Lynch, et al., Preliminary evaluation of the feasibility of using polypropylene fibres from COVID-19 single-use face masks to improve the mechanical properties of concrete, J. Clean. Prod. 296 (2021), 126460.
[13] L. Ajam, A. Trabelsi, Z. Kammoun, Valorisation of face mask waste in mortar, Innovate. Infrastruct. Sol. 7 (1) (2022) 1–10.
[14] W. Gao, et al., The status, challenges, and future of additive manufacturing in engineering, Comput. Aided Des. 69 (2015) 65–89.
[15] T. Wangler, et al., Digital concrete: a review, Cement Concr. Res. 123 (2019), 105780.
[16] V.N. Nerella, S. Hempel, V. Mechtcherine, Effects of layer-interface properties on mechanical performance of concrete elements produced by extrusion-based 3D-printing, Construct. Build. Mater. 205 (2019) 586–601.
[17] B. Panda, S.C. Paul, M.J. Tan, Anisotropic mechanical performance of 3D printed fiber reinforced sustainable construction material, Mater. Lett. 209 (2017) 146–149.
[18] M. Hambach, M. Rutzen, D. Volkmer, Properties of 3D-printed fiber-reinforced Portland cement paste, in: 3D Concrete Printing Technology, Elsevier, 2019, pp. 73–113.
[19] S. Luhar, et al., Sustainable and renewable bio-based natural fibres and its application for 3D printed concrete: a review, Sustainability 12 (24) (2020), 10485.
[20] A. Perrot, D. Rangeard, A. Pierre, Structural built-up of cement-based materials used for 3D-printing extrusion techniques, Mater. Struct. 49 (4) (2016) 1213–1220.
[21] A.R. Arunothayan, et al., Rheological characterization of ultra-high performance concrete for 3D printing, Cement Concr. Compos. 136 (2023), 104854.
[22] S. Hou, et al., A review of 3D printed concrete: Performance requirements, testing measurements and mix design, Constr. Build. Mater. 273 (2021) 121745.
[23] J. Sanjayan, R. Jayathilakage, P. Rajeev, Vibration induced active rheology control for 3D concrete printing, Cement Concr. Res. 140 (2021), 106293.
[24] R. Jayathilakage, P. Rajeev, J. Sanjayan, Yield stress criteria to assess the buildability of 3D concrete printing, Construct. Build. Mater. 240 (2020), 117989.
[25] J. Xiao, et al., Rheology of 3D printable concrete prepared by secondary mixing of ready-mix concrete, Cement Concr. Compos. (2023) 104958.
[26] G. Moelich, P. Kruger, R. Combrinck, Mitigating early age cracking in 3D printed concrete using fibres, superabsorbent polymers, shrinkage reducing admixtures, B-CSA cement and curing measures, Cement Concr. Res. 159 (2022), 106862.
[27] J. Van Der Putten, et al., Development of 3D printable cementitious composites with the incorporation of polypropylene fibers, Materials 14 (16) (2021) 4474.
[28] M.V. Tran, Y.T. Cu, C.V. Le, Rheology and shrinkage of concrete using polypropylene fiber for 3D concrete printing, J. Build. Eng. 44 (2021), 103400.
[29] L. Ma, et al., Pore structure, internal relative humidity, and fiber orientation of 3D printed concrete with polypropylene fiber and their relation with shrinkage, J. Build. Eng. 61 (2022), 105250.
[30] Standard, A., AS 3972 General Purpose and Blended Cements, Australian Standard, 2010.
[31] Standard, A., AS 3582.3 Supplementary Cementitious Materials for Use with Portland and Blended Cement, Australian Standard, 2016.
[32] ASTM, I., ASTM C136 Standard Test Method for Sieve Analysis of Fine and Coarse Aggregates, ASTM International, West Conshohocken, PA, 2006.
[33] Standard, A., AS 1478.1 Chemical Admixtures for Concrete, Mortar and Grout-admixtures for Concrete, Asustralian Standard, 2000.
[34] Astm, D., ASTM D5035-11 Standard Test Method for Breaking Force and Elongation of Textile Fabrics (Strip Method), ASTM Standards, 2019.
[35] https://danishfibres.com/wp-content/uploads/2020/12/2020_10_18_Wiking_18_my_EN.pdf.
[36] A.R. Arunothayan, et al., Fiber orientation effects on ultra-high performance concrete formed by 3D printing, Cement Concr. Res. 143 (2021), 106384.
[37] Y. Yang, et al., Mechanical anisotropy of ultra-high performance fibre-reinforced concrete for 3D printing, Cement Concr. Compos. 125 (2022) 104310.
[38] A. de la Fuente, et al., Structural fibre-reinforced cement-based composite designed for particle bed 3D printing systems. Case study Parque de Castilla Footbridge in Madrid, Cement Concr. Compos. 157 (2022) 106801.
[39] ASTM, I., ASTM C1437 Standard Test Method for Flow of Hydraulic Cement Mortar, ASTM International, 2007.
[40] D. Feys, et al., Extension of the Reiner–Riwlin equation to determine modified Bingham parameters measured in coaxial cylinders rheometers, Mater. Struct. 46 (1) (2013) 289–311.
[41] S. Fataei, E. Secrieru, V. Mechtcherine, Experimental insights into concrete flow-regimes subject to shear-induced particle migration (SIPM) during pumping, Materials 13 (5) (2020) 1233.
[42] S. Muthukrishnan, S. Ramakrishnan, J. Sanjayan, Effect of alkali reactions on the rheology of one-part 3D printable geopolymer concrete, Cement Concr. Compos. 116 (2021), 103899.
[43] S. Muthukrishnan, S. Ramakrishnan, J. Sanjayan, In-line activation of geopolymer slurry for concrete 3D printing, Cement Concr. Res. 162 (2022), 107008.
[44] J. Assaad, K.H. Khayat, H. Mesbah, Assessment of thixotropy of flowable and self-consolidating concrete, Mater J. 100 (2) (2003) 99–107.

[45] P.V. Liddel, D.V. Boger, Yield stress measurements with the vane, J. Non-Newtonian Fluid Mech. 63 (2–3) (1996) 235–261.
[46] F.P. Bos, et al., Juxtaposing fresh material characterisation methods for buildability assessment of 3D printable cementitious mortars, Cement Concr. Compos. 120 (2021), 104024.
[47] J. Kruger, et al., 3D concrete printer parameter optimisation for high rate digital construction avoiding plastic collapse, Compos. B Eng. 183 (2020), 107660.
[48] S. Ramakrishnan, S. Kanagasuntharam, J. Sanjayan, In-line activation of cementitious materials for 3D concrete printing, Cement Concr. Compos. (2022), 104598.
[49] D. Lootens, et al., Yield stress during setting of cement pastes from penetration tests, Cement Concr. Res. 39 (5) (2009) 401–408.
[50] J.G. Sanjayan, et al., Effect of surface moisture on inter-layer strength of 3D printed concrete, Construct. Build. Mater. 172 (2018) 468–475.
[51] S. Muthukrishnan, S. Ramakrishnan, J. Sanjayan, Effect of microwave heating on interlayer bonding and buildability of geopolymer 3D concrete printing, Construct. Build. Mater. 265 (2020), 120786.
[52] ASTM, I., ASTM C642 Standard Test Method for Density, Absorption, and Voids in Hardened Concrete, ASTM International, 2013.
[53] A.R. Arunothayan, et al., Digital fabrication of eco-friendly ultra-high performance fiber-reinforced concrete, Cement Concr. Compos. 125 (2022), 104281.
[54] K. Zhang, et al., How does adsorption behavior of polycarboxylate superplasticizer effect rheology and flowability of cement paste with polypropylene fiber? Cement Concr. Compos. 95 (2019) 228–236.
[55] S. Shyshko, Numerical Simulation of the Rheological Behavior of Fresh Concrete, TU Dresdan, 2013.
[56] M. Chen, et al., Rheological behaviors and structure build-up of 3D printed polypropylene and polyvinyl alcohol fiber-reinforced calcium sulphoaluminate cement composites, J. Mater. Res. Technol. 10 (2021) 1402–1414.
[57] K.H. Khayat, et al., Rheological properties of ultra-high-performance concrete—an overview, Cement Concr. Res. 124 (2019), 105828.

Update

Cement and Concrete Composites
Volume 152, Issue , September 2024, Page

DOI: https://doi.org/10.1016/j.cemconcomp.2024.105649

Cement and Concrete Composites 152 (2024) 105649

Contents lists available at ScienceDirect

Cement and Concrete Composites

journal homepage: www.elsevier.com/locate/cemconcomp

Erratum to “Using fibre recovered from face mask waste to improve printability in 3D concrete printing” [Cement Concr. Compos. 139 (2023) 105047]

Pathmanathan Rajeev [a,*], Akilesh Ramesh [a], Satheeskumar Navaratnam [b], Jay Sanjayan [a]

[a] Centre for Sustainable Infrastructure and Digital Construction & Department of Civil and Construction Engineering Swinburne University of Technology, Hawthorn, VIC, Australia

[b] School of Engineering, RMIT University, Australia

The publisher regrets a production error in Section 3.1, paragraph 2, Line 1, where “360 mm × 400 mm” should be “360 mm × 420 mm”. The publisher would like to apologise for any inconvenience.

DOI of original article: https://doi.org/10.1016/j.cemconcomp.2023.105047.

* Corresponding author.
E-mail address: prajeev@swin.edu.au (P. Rajeev).

https://doi.org/10.1016/j.cemconcomp.2024.105649

Available online 2 July 2024